Environmental Modelling and Software xxx (xxxx) 105043

Contents lists available at ScienceDirect

Environmental Modelling and Software

journal homepage: www.elsevier.com/locate/envsoft

Towards a global Reservoir Assessment Tool for predicting hydrologic impacts and operating patterns of existing and planned reservoirs

Nishan Kumar Biswas [a], Faisal Hossain [a,*], Matthew Bonnema [b], Hyongki Lee [c], Farrukh Chishtie [d,e]

[a] Department of Civil and Environmental Engineering, University of Washington, Seattle, WA, USA
[b] Postdoctoral Scholar, Earth Sciences Division, Jet Propulsion Laboratory, NASA, CA, USA
[c] Department of Civil and Environmental Engineering, University of Houston, Houston, TX, USA
[d] SERVIR-Mekong, Asian Disaster Preparedness Center (ADPC), Bangkok, Thailand
[e] Spatial Informatics Group, LLC, 2529 Yolanda Ct., Pleasanton, CA, 94566, USA

ARTICLE INFO

Keywords:
Reservoir monitoring
Satellite remote sensing
Landsat
Global hydrology

ABSTRACT

Dam construction in developing nations is on the rise. Monitoring these dams is essential to understanding downstream hydrologic impacts and for better planning and management of water resources. Satellite observations and advancements in information technology now present a unique opportunity to overcome the traditional limitations of reservoir monitoring. In this study, a global reservoir monitoring framework was developed as an online tool for near real-time monitoring and impact analysis of existing and planned reservoirs based on publicly available and global satellite observations. The framework used a mass balance approach to monitor 1598 reservoirs in South America, Africa, and Southeast Asia. Simulated streamflow of the developed tool was validated in 25 river basins against a multidecadal record of in-situ discharge. The simulated storage change was validated against in-situ data from 77 reservoirs. The framework was able to capture reservoir state realistically for more than 75% of these reservoirs. At most in-situ gaging locations, the reservoir tool was able to capture streamflow with a correlation of more than 0.9 and a normalized root mean square error of 50% or less. The tool can now be used to study existing or planned reservoirs for short and long-term decision making and policy analysis.

1. Introduction

By the end of the 20th century, approximately 58,000 large dams higher than 15 m, with a total reservoir surface area of about 300,000 km^2 (Lehner et al., 2011) had been built for hydroelectricity, irrigation, and water supply needs. With rapid growth in human population and energy demand, dam construction in the developing world is currently rising (Zarfl et al., 2014). The majority of dams either planned or already under construction are concentrated in South America, Asia, and Africa, mainly in developing countries with Human Development Index values ranging from "low to medium," as defined by the United Nations Development Program (Fig. 1). Many of these new or upcoming dams are designed to harness the hydropower potential of rivers and to supply water for drinking and irrigation.

Dams and reservoirs have long been treated as cheap and clean energy sources with low carbon emissions and benefits related to flood control, food security, irrigation, and socio-economic development. Hereafter, dams and reservoirs will be used interchangeably in this paper. For example, dams built for irrigation purposes provide water to 30–40% of the world's agricultural lands and produce about 40% of the world's food (World Bank, 2020). Dams also have long-term downstream consequences due to disruptions they pose to the natural flow regime. Flow regulation and river fragmentation (Bunn and Arthington, 2002), narrowing of river beds and downstream erosion (Khan et al., 2014), seawater intrusion (Sikder, 2013), and thermal stratification (Lugg and Copeland, 2014) are among the many ways dams negatively impact river systems. Grill et al. (2015) studied existing and future large dams, showed a 48% alteration of rivers, and predicted that the number could rise to 93% if all planned dams are built. Unplanned and uncoordinated dam management also affects downstream flooding (Mishra and Shah, 2018), disrupts pre-existing agriculture production (Strobl and Strobl, 2011), and weakens the ecosystem (Poff and Zimmerman, 2010). Due to significant impacts of dams on the environment, it is necessary for all basin inhabitants, particularly

* Corresponding author. Department of Civil and Environmental Engineering, Wilcox 167, Box: 352700, University of Washington, Seattle, WA, 98195, USA.
E-mail address: fhossain@uw.edu (F. Hossain).

https://doi.org/10.1016/j.envsoft.2021.105043
Accepted 28 February 2021
1364-8152/

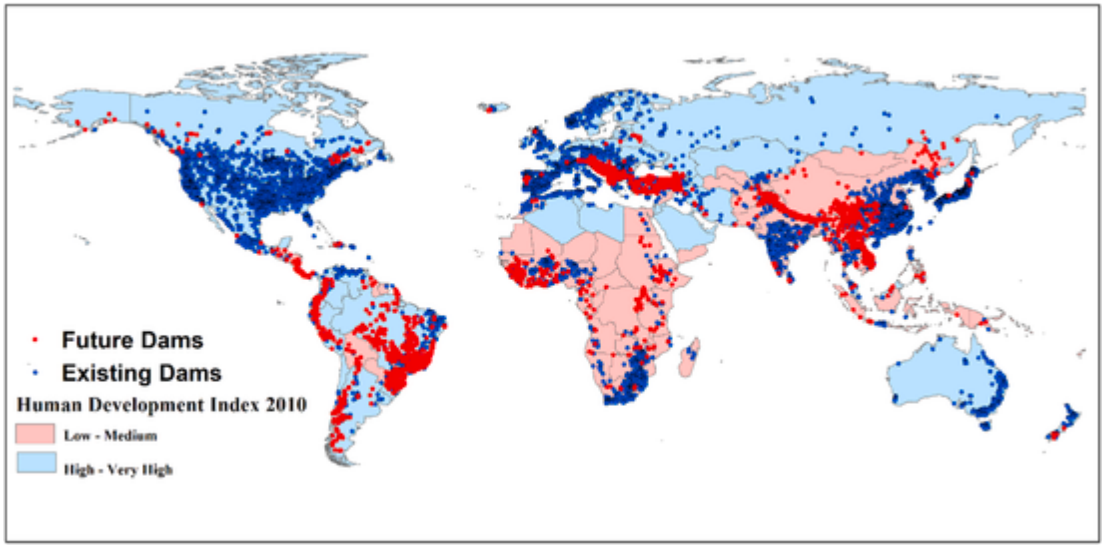

Fig. 1. Overview of 6862 large dams (Lehner et al., 2011) and about 3700 planned and under-construction hydropower dams with an installed capacity > 1 MW (Zarfl et al., 2014). The map: United Nations' Development Program's Human Development Index for 2010.

those living downstream, to understand the operating pattern and state of upstream reservoirs.

Downstream nations, as well as all riparian nations, can make both immediate and long-term decisions for water management and maximize stakeholder benefits, through the unhindered exchange of hydrologic data and reservoir-operating information. Understanding the role dams play in flow regimes is also necessary to manage water-related hazards such as floods and droughts, public safety and infrastructure resilience (Woldemichael et al., 2012), effects of human alterations to the land hydrologic cycle (Gao et al., 2012), and impacts of multi-reservoir systems on downstream river discharge (Döll and Zhang, 2009). It is also critical to know how reservoir operating patterns will need to be revised to address climate change, especially in climate-vulnerable regions such as the Amazon (Pokhrel et al., 2014) and the Mekong basin (Lauri et al., 2012). Despite clear need and urgent calls for the unhindered exchange of hydrologic information (Khattar and Ames, 2020), global and freely accessible reservoir monitoring information is currently unavailable for inhabitants of regulated basins around the world. This is due to insufficient ground observations, particularly in developing regions, limited data sharing protocols (Alsdorf et al., 2007; Hossain et al., 2007) and lack of financial resources (Solander et al., 2016a,b). Such hurdles make it challenging to study and routinely monitor the impact of reservoirs around the world (Gao et al., 2012).

Due to the absence of direct measurements, models have been used to monitor reservoirs at the continental and global scale, as well as to assess future climate projections (Döll et al., 2003, 2009; Hanasaki et al., 2006; Meigh et al., 1999). However, large-scale modeling approaches do not accurately resolve individual dams, making them less relevant for local decision-makers. When global reservoir modeling systems were still in the early stages of development, it was often assumed that a rectangular or inverse pyramid-shaped bathymetry would represent the storage capacity of reservoirs (Döll et al., 2003; Meigh et al., 1999). The first grid-based, explicit representation of a reservoir used in global hydrological models was reported by Hanasaki et al. (2006) and subsequently improved by several other studies (Pokhrel et al., 2014; Voisin et al., 2013). Solander et al. (2016a,b) proposed a very idealized reservoir model by using temperature as the primary factor to simulate seasonal changes in reservoir management. Despite the above-mentioned modeling studies used to simulate the effect of dams on river discharge, several issues remain unsolved relating to spatiotemporal dynamics of the individual reservoir (Bierkens et al., 2015). For example, most schemes were developed for macroscale hydrologic models with typical grid sizes of more than 50 km (Fatichi et al., 2016), which is unsuitable for representing small to medium-sized reservoirs. Also, none of the studies considered reservoir surface area dynamics and bathymetry, which is critical to capturing reservoir evaporation and impacts on the weather (Degu et al., 2011).

The calibration and validation of most global models were completed using in-situ observations from developed regions. Thus, the skill of such modeling systems remained untested for operational decision-making and policy analysis in developing regions (Gao et al., 2012). Most recently, Yigzaw et al. (2018) proposed a method to define a characteristic shape of the reservoir for an area-elevation relationship that facilitates easier software representation of reservoir bathymetry in earth system models that also works well for reservoir related studies. However, every reservoir is unique in its bathymetry, and defining an idealized shape may not be suitable for deriving skillful storage change or detecting reservoir operating patterns for the individual dam. Thus, to reduce uncertainties related to the actual representation of reservoir topography along with surface area dynamics in global monitoring, satellite remote sensing is needed that can measure or estimate a wide range of variables and provide data to determine a reservoir's state.

Over the last few decades, satellite remote sensing has played an important role in providing spatio-temporal observations of surface water and hydrologic processes at global-scale coverage with near real-time availability (Khaki et al., 2020; Biswas and Hossain, 2017; Avisse et al., 2017; Kansakar and Hossain, 2016; Gebregiorgis and Hossain, 2011). The application potential of remote sensing observations for deriving reservoir state and operating patterns has been well established in previous studies (Bonnema et al., 2016; Gao et al., 2012). The same approach used in Bonnema et al. (2016) was later applied to over 20 reservoirs of the Mekong Basin to infer the operating pattern of reservoirs and residence time (Bonnema and Hossain, 2017; Hossain et al., 2019). However, such approaches have so far been limited to individual regions or reservoirs. With the availability of remotely sensed observations and computationally robust and versatile online software tools (such as cloud and distributed computing), it is now possible to have a global scale and freely accessible monitoring framework for existing and planned reservoirs (Wood et al., 2011).

In order to build an online, global-scale reservoir framework for information monitoring, several priority issues must be addressed. These issues include the following: (1) automatic delineation of spatial extent around the reservoir shoreline to derive the dynamic surface area, commonly known as the region of interest (ROI); (2) construction of the

area-elevation relationship to define reservoir bathymetry; (3) selection of a universally applicable method to estimate the time series of the reservoir's water surface area; (4) setup and calibration of the upstream hydrological model to derive reservoir inflow; (5) advanced understanding of remote sensing, models and data for the users; and (6) availability of computational resources. With the availability of the GranD Dam Database (Lehner et al., 2011), a georeferenced reservoir database is now available for global-scale studies. This database, however, does not provide all necessary information on reservoirs, such as the maximum areal extent of reservoir or ROI. In previous studies (Gao et al., 2012; Bonnema et al., 2016), the ROI had been manually identified using the visible/Infrared imageries. Some studies (i.e., Zhao and Gao, 2018) used a fixed buffering distance around a reservoir polygon for defining ROI for global-scale studies, which may not yield accurate results for reservoirs that are highly irregular in shape.

The extraction of reservoir surface area poses the most difficult challenge in obtaining a globally scalable method. There are numerous studies (Bonnema and Hossain, 2017; Gao, 2015; Pekel et al., 2016; Zhao and Gao, 2018) related to water area extraction of lakes and reservoirs using different passive and active satellite sensors (i.e., Landsat 5,7, 8, Sentinel 1 and 2). The calculation of reservoir inflow on a global scale is another critical issue. There is no global parameterization for any of the hydrological models that can be applied universally. Nijssen et al. (2001a,b) optimized the Variable Infiltration Capacity (VIC) model parameters at the global scale to estimate global river discharge and sensitivity to climate change. However, the spatial resolution is too coarse for most reservoirs, and the approach lacks a streamflow routing model. There are a number of other streamflow datasets and global hydrological modeling frameworks (Lin et al., 2019; Barbarossa et al., 2018) that exist based on global hydrological model setups. Two major limitations with any dataset are the lack of publicly accessible operational modeling at a daily or weekly timescale and datasets with spatial resolution that is too coarse to capture the dynamics of reservoirs of all sizes. Thus, routine monitoring of reservoirs in near real-time that is also publicly accessible cannot be achieved with existing hydrological models and frameworks. Even if all the above constraints were addressed, an advanced understanding of remote sensing and modeling would still be required for stakeholders from developing countries wishing to manage their river basins under increasing transboundary regulation. Fortunately, there have been recent technological advancements, including the publicly available cloud, which can now eliminate many of the limitations faced by inhabitants of developing nations. Another advancement is distributed computing that reduces the requirement of high internet bandwidth for downloading and processing of large-scale datasets. For example, Google Earth Engine (GEE) (Gorelick et al., 2017) combines a multi-petabyte catalog of satellite imagery and geospatial datasets with the planetary-scale analysis that has been applied in several studies of reservoirs (Biswas et al., 2019; Bonnema and Hossain, 2017; Zhao and Gao, 2018).

This study describes an operational framework for developing the software needed for a global, freely available monitoring system of reservoirs in developing regions. This modeling framework, known as Reservoir Assessment Tool (RAT), is motivated by the need to democratize access to information on reservoir operations and study reservoir impacts on hydrology so that inhabitants and water managers can devise 21st-century solutions. Those end users who lack advanced knowledge of remote sensing, access to in-situ or transboundary data, or the capacity to operate complex hydrological models will find such a software tool useful in their efforts to monitor and manage their reservoirs.

The study describing the development of RAT is organized as follows. First, the reservoir mass balance approach used in RAT is shown in Section 2.1, with datasets described in Section 2.2. Using these datasets, the specific methods used to estimate different parameters of reservoir states are described in Section 2.3. The user interface and overview of the proposed operational framework are briefly described in Section 3. Validation results for the RAT framework are presented in Section 4, where accuracy of the simulated storage change, surface area estimation, and reservoir inflow is assessed against reference data. The conclusion and scope for further development of the RAT framework are described in Section 5.

2. Framework description

2.1. Overview and reservoir mass balance approach

In this study, satellite-based remote sensing data were used to estimate reservoir outflow by employing a reservoir mass balance equation (1). For monitoring reservoir dynamics (fill, release and storage change), this mass balance is the core component of the RAT framework. A schematic diagram of the mass balance concept is shown in Fig. 2.

$$O = I - E - \Delta S \tag{1}$$

Here, the terms represent the following: O = Outflow, I = inflow, E = Evaporative loss, and ΔS = Storage change. In this study, the term "outflow" was used as a proxy for "release," which also included parallel diversions and other consumptive uses. The reservoir surface water extent areas A_{t-1} and A_t in Fig. 2 were extracted from visible/NIR imageries, corresponding heights h_{t-1} and h_t were extracted using Area-Elevation Curve (AEC), and finally, ΔS was calculated using equation (2). Details about the AEC development are discussed in Section 2.3.2.

$$\Delta S = \frac{A_{t-1} + A_t}{2} * (h_t - h_{t-1}) \tag{2}$$

First, the ROI (previously explained in the Introduction section) of any reservoir is defined by following a reservoir size-dependent buffer distance shown in Table 1. The ROI is used to clip satellite observations for preparing the area-elevation relationship and to extract the time series of surface water area. Storage change of any reservoir can be computed using the reservoir water surface area/elevation time series and area-elevation relationship shown in Fig. 2. This is a widely-used technique that has been reported to yield acceptable skill (Bonnema et al., 2016; Crétaux et al., 2011; Gao, 2015; Gao et al., 2012). Meteorological observations and land surface parameters are forced into a hydrological model to derive reservoir inflow. The inflow, evaporation, and storage change can then be used to infer the reservoir outflow using mass balance. Details about the datasets and specific methods are discussed in Sections 2.2, 2.3, and 2.4.

2.2. Datasets

The land elevation dataset used in this study was the Shuttle Radar Topography Mission (SRTM) 30 m resolution Digital Elevation Model (DEM) (Hennig et al., 2001). Three sensors were used to derive water-extent area time series, including (1) USGS Landsat 8 Collection 1 Tier 1 and Real-Time data Raw Scenes, (2) Sentinel-1 SAR GRID: C-band Synthetic Aperture Radar Ground Range Detected, and (3) Sentinel-2 MSI: Multispectral Instrument, Level-1C. In the gridded hydrological model, FAO Harmonized World Soil Database (Nachtergaele et al., 2008), USGS Global Land Cover Characteristics (GLCC), and Land Cover Database (Geological Survey, 1997) were used for land-surface parameters. CHIRPS precipitation (Funk et al., 2015), maximum and minimum temperature, and average wind speed at 10 m height from NOAA NCEP/Climate Prediction Center provided meteorological forcing data for this study. For routing the hydrological model outputs, global flow direction at 1/16° spatial resolution (Wu et al., 2011) was used.

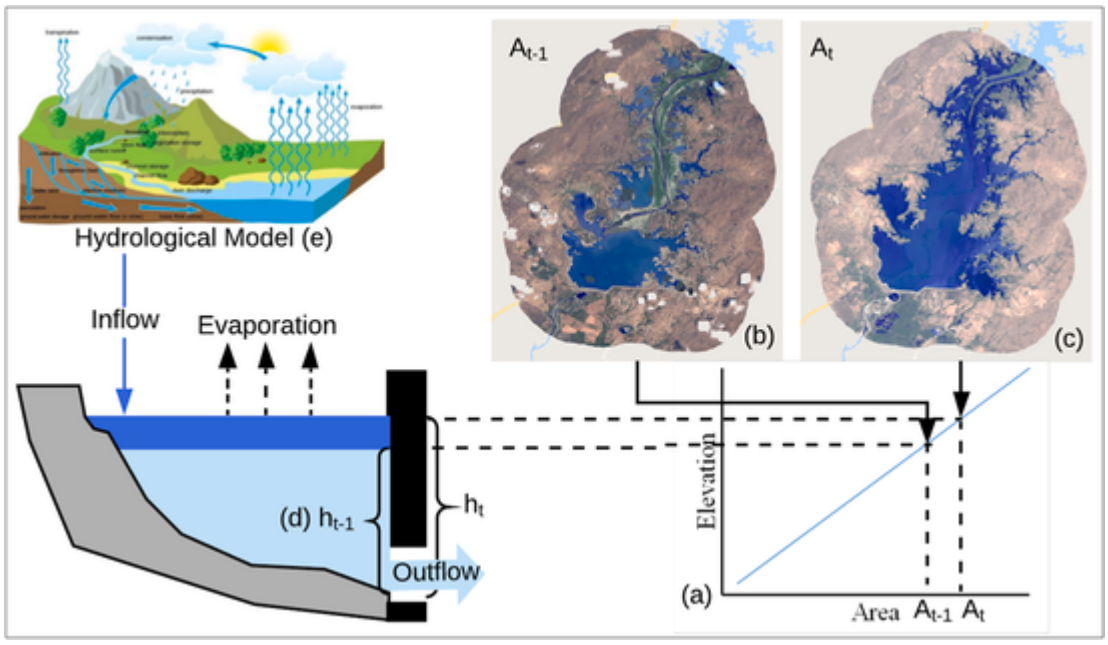

Fig. 2. Concept of satellite data-based mass balance for reservoir monitoring. The reservoir parameters and corresponding satellite datasets used are as follows: (a) The Area-Elevation relationship Curve (AEC) derived from SRTM, (b) and (c) are from visible/NIR satellite imagery, (d) was derived from AEC and (e) from satellite-based meteorological observations.

Table 1
Reservoir class, buffering distance, and computational scale in GEE.

Reservoir Surface Area from GranD (Km^2)	Buffering Distance (m)
<2.0	500
2–10	750
10–50	1000
50–200	1250
200–500	1500
500–1000	1750
>1000	2000

2.3. Storage change calculation

The method followed in this study to calculate change in reservoir storage is shown in Fig. 2. Major components mentioned in the mass balance equation are (a) ROI generation, (b) AEC extraction, (c) time-series processing of water extent area, (d) storage change calculation, (e) simulation of reservoir inflow from the hydrological model and evaporation from the reservoir, and (f) reservoir outflow calculation. Aside from hydrologic modeling (items e and f), all components are executed in the cloud using Google Earth Engine (GEE) to minimize internet bandwidth needed for downloading large datasets. GEE has been extensively used in different large-scale hydrological analyses (Biswas et al., 2019; Pekel et al., 2016; Zhao and Gao, 2018), which offers highly advanced and previously unachievable computational possibilities.

2.3.1. ROI delineation

After many trials over several reservoirs using multiple approaches, we classified the reservoirs according to the polygon defined in the GranD database. The polygon area was used to classify reservoirs into seven distinct classes to identify the appropriate buffering distance to create the ROI. Before deciding the buffering distance for each class, the frequency of occurrence map of the global surface water dataset (GSWD) prepared by Pekel et al. (2016) was used for visual comparison over 70–80 reservoirs. By following the maximum water extent of the GSWD dataset, a suitable buffer distance was decided (Table 1).

2.3.2. Area-elevation curve extraction

Using the delineated ROI mentioned in Section 2.3.1 and SRTM DEM data, the Area Elevation Curve (AEC) was derived in two steps. First, the ROI of the selected reservoir was used to clip the SRTM DEM. The SRTM DEM elevation was used to generate the area-elevation relationship, which was valid for elevation above the water surface at the time of the SRTM overpass (which was in February 2000). The histogram of SRTM DEM was populated to count the number of cells corresponding to each of the elevation data. The area of individual elevation was then calculated and incremented to get incremental area. The steepest slope of the AEC was used to identify elevations corresponding to reservoir surface areas. Areas less than the area of water surface elevation were considered to be satellite noise and discarded from further analysis. Next, the relationship developed in the first step was extrapolated to the near-zero surface area in order to complete a virtual area-elevation relationship for elevations lower than the SRTM-observed water surface. During extrapolation, univariate spline was found to be the best estimator and was therefore used as the operational area-elevation relationship generator. Finally, these two area-elevation relationships were merged to create the complete area-elevation curve. The whole methodology of AEC development is summarized graphically in Fig. 3. For more information on the area-elevation curve generation approach, readers are referred to the works of Bonnema et al. (2016) and Bonnema and Hossain (2017).

2.3.3. Surface water area extraction

The surface area time series and the AEC are prerequisites to calculating the storage change of any reservoir. First, the ROI polygon and AEC are prepared by following the approach mentioned in Sections 2.2.1 and 2.2.2. All imagery scenes are first filtered using a predefined date window and the ROI polygon, and then clipped using the ROI. In the case of Sentinel 2 and Landsat, cloudy pixels were removed from the ROI region of the scene. The area of scenes was calculated and filtered out for areas less than 80% of the ROI (after the removal of cloudy and partially covered scene). In the case of Sentinel 1, scenes were filtered based on polarization, look angle, and date window, and pixels with less than −16 dB backscatter value (Ahmad et al., 2019) were treated as water. For Landsat and Sentinel 2, different index-based methods

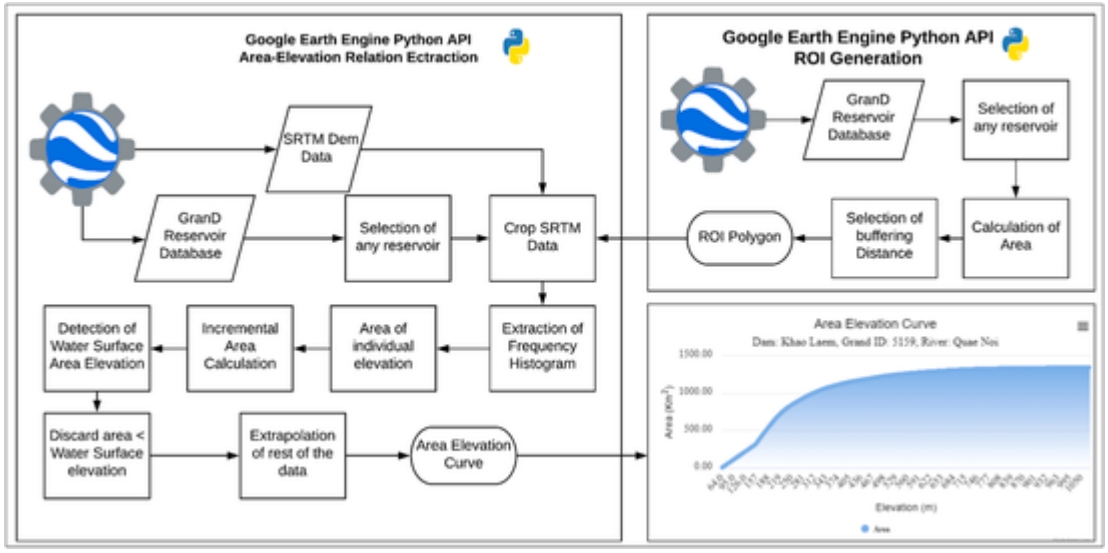

Fig. 3. Reservoir ROI polygon delineation and AEC curve extraction procedure.

were assessed, such as Normalized Difference Water Index-NDWI (McFeeters, 1996), Modified Normalized Difference Water Index-MNDWI (Xu, 2006), Water Index (Fisher et al., 2016), Advanced Water Extraction Index (Feyisa et al., 2014), and Dynamic Surface Water Extent-DSWE (Jones, 2019). The extracted time series were then used to calculate the storage change time series (Fig. 4).

2.3.4. Calculating storage change

The storage change time series was calculated from the surface time series of the water extent area and the AEC (Fig. 4). For any pair of consecutive surface-water area data, corresponding elevations were computed from the AEC. Storage change was calculated from two consecutive heights and elevations using equation (2).

2.4. Simulation of reservoir inflow

The reservoir inflow was simulated using a hydrological model with streamflow routing capability. Variable Infiltration Capacity (VIC) model (Liang et al., 1994; Lohmann et al., 1998) was chosen for simulating the gridded surface runoff, evaporation, and baseflow in the upstream catchment area of the reservoir. Meteorological observations forced the model, along with land-surface parameters. For soil and land surface parameters, FAO land cover and World Harmonized Soil Dataset were used. Meteorological parameters used in this study were precipitation, maximum and minimum temperature, and average wind speed. All input forcings to the VIC model were prepared at 0.0625° by 0.0625° spatial resolution to match the Dominant River Tracing (DRT) flow direction at 0.0625° resolution (Wu et al., 2011). We chose the finest resolution of the hydrological model and DRT flow direction to

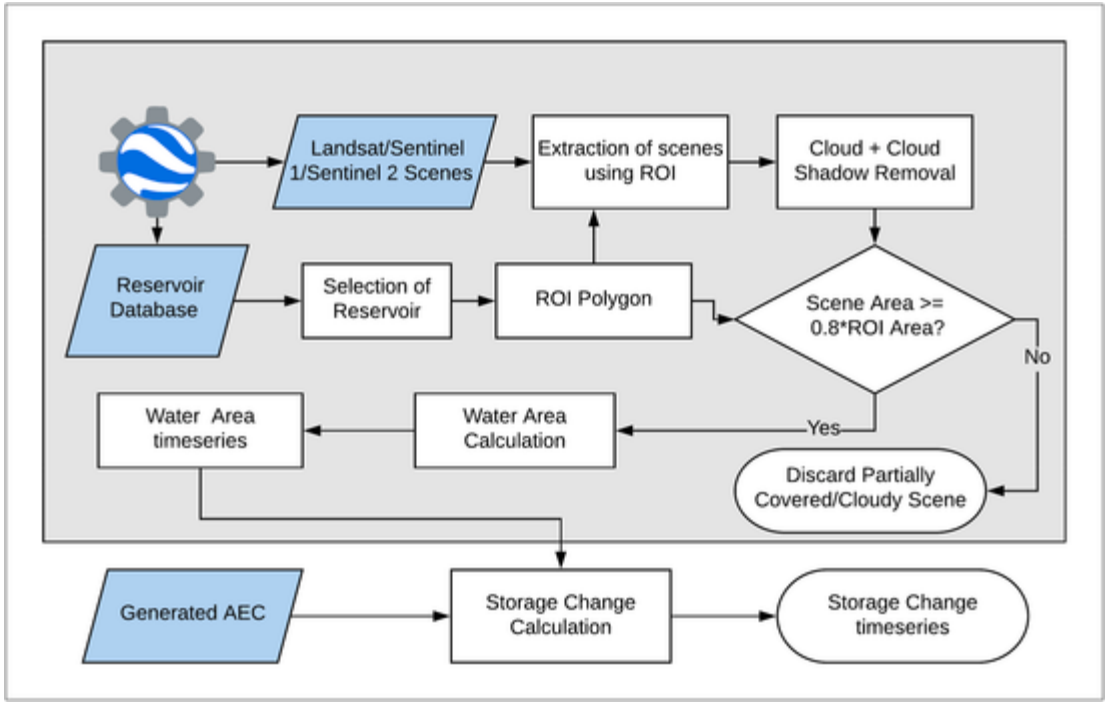

Fig. 4. Workflow for surface water area time series and storage change.

cover the maximum number of reservoirs possible from the GranD database (Lehner et al., 2011).

There are several calibration parameters for the VIC model, which can be used to improve simulated streamflow. Some of these parameters (i.e., saturated hydraulic conductivity and the exponent of the unsaturated hydraulic conductivity curve) were estimated from soil properties by following the approach mentioned in Nijssen et al. (2001a,b). Initially, the two calibration parameters (variable infiltration parameter and depth of the soil layer) were taken from Nijssen et al. (2001a,b). We found that those critical parameters identified in Nijssen et al. (2001a,b) were thoroughly investigated, based on climatic zone and geographical region, and presented the best available baseline study. These calibration parameters were resampled to a spatial resolution of 0.0625° by 0.0625° by using the cubic spline interpolation technique. The calibrated parameters were further updated wherever it was available to ensure better estimation of reservoir inflow by following more recent studies in several basins. For example, we used parameters for Ganges, Brahmaputra, Meghna basins from Siddique-E-Akbor et al. (2014), for Indus basin from Iqbal et al. (2017), for Mekong basin from Hossain et al. (2017) and for Nile basin from Eldardiry and Hossain (2019).

Upon completion of hydrological model simulation, outputs were forced into the Routing Model (Lohmann et al., 1998) along with the DRT flow direction (Wu et al., 2011) to simulate reservoir inflow. DRT flow-direction-derived flow accumulation was matched with satellite imagery and river networks manually in most of the reservoir locations. It was done by comparing the flow accumulation from the DRT flow direction to satellite imagery at different locations with the assistance of Google Earth (https://www.google.com/earth/).

2.4.1. Calculation of reservoir evaporation and outflow

The total net evaporation computed by the VIC hydrological model was used to compute the evaporation from the reservoirs. Users are referred to https://vic.readthedocs.io for a detailed description of total net evaporation calculation of VIC Model. Here, the VIC model grid closest to the dam location was identified, and the simulated total net evaporation at that grid cell was assumed to represent reservoir surface evaporation over a unit area. This amount of evaporation from the grid cell was multiplied by the reservoir surface area to calculate the evaporation from the reservoir. Equation (1) was used to calculate outflow from the reservoir. The inflow volume, storage change volume, and evaporation amount were used to calculate outflow volume between two consecutive storage changes. We have assumed the role of seepage and groundwater loss as minor, based on a previous study (Bonnema et al., 2016), and thus discarded them from the mass balance approach.

2.4.2. Consideration of upstream reservoirs

Where there is a series of reservoirs along a river and its tributaries and the inflow volume of the upstream reservoir is greater than 10% of the natural inflow to the downstream reservoir, the influence of the upstream reservoir on downstream inflow was considered. This was done by deriving the difference between the inflow and outflow of the upstream reservoir and adjusting for that for downstream reservoir inflow.

3. The interface of Reservoir Assessment Tool (RAT) and operational reservoir monitoring

3.1. Graphical user interface (GUI)

The main window of the frontend is shown in Fig. 5, which can be accessed through http://depts.washington.edu/saswe/rat_beta. The detailed design of the frontend and salient features of the tool are discussed in the user manual of the tool and also available in the GitHub link (https://github.com/nbiswasuw/rat-reservoir_assessment_tool). Currently, 1598 Dams from the GranD Database version 1.3 located in South America, Africa, and Southeast Asia are modeled operationally and visualized on the RAT frontend interface. All reservoir parameters (i.e., AEC, surface water extent, inflow, storage change, and outflow) were added to the frontend.

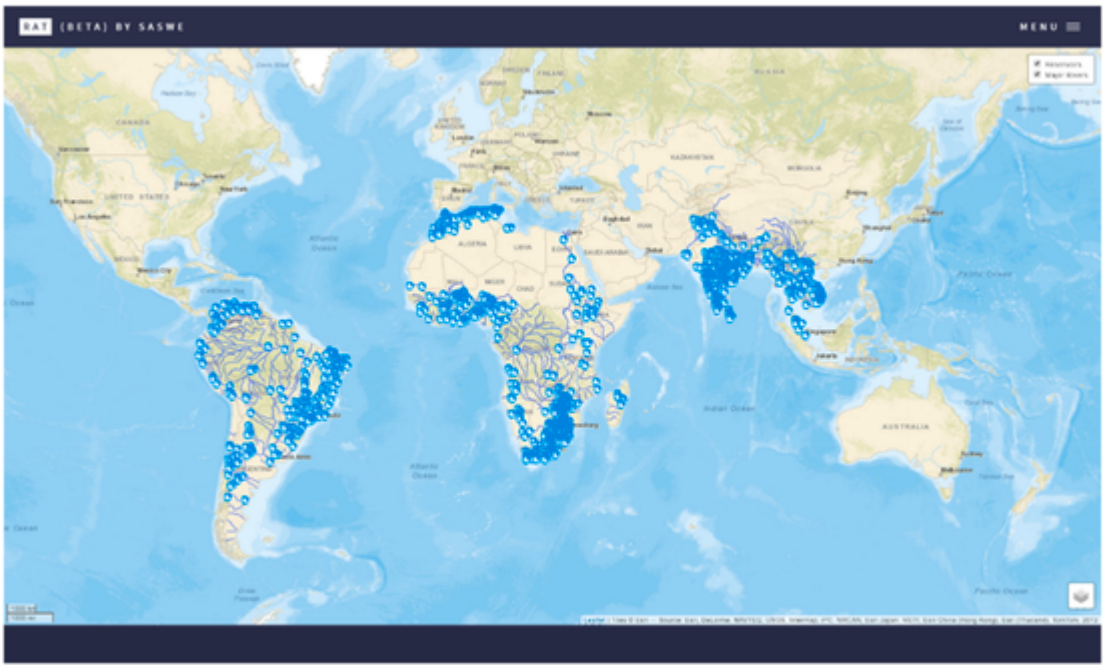

Fig. 5. Frontend web interface of the RAT tool operational framework with the blue reservoir icons showing reservoir locations. The polylines are the river network downloaded from https://www.naturalearthdata.com. The upper right corner of the window allows users to toggle between selections of layers and to switch available basemaps from the lower right corner.

3.2. Monitoring of reservoirs

3.2.1. Monitoring of existing reservoirs

As more recent and frequent satellite observations on reservoir areas become available via GEE, the RAT framework automatically processes the data, runs the hydrological model, and post-processed model outputs to create updated estimates of outflow, inflow, storage change of the existing reservoirs. The water extent time series is extracted with the latest available scenes per the methodology used for water-extent area extraction, mentioned in Section 2.3.3. The available AEC data and water extent time series are processed to get the storage change time series. VIC model is simulated weekly (at a daily time step) to get the most recent inflow into the reservoirs. Finally, the outflow is calculated from the inflow and storage change. All of these time-series data are made available in the frontend for user access. The data and information interchange between the backend server and the frontend GUI of the tool is explained in Fig. 6. If the inflow into any reservoir is not calculated, the user can make a request through the frontend, which is explained next in Section 3.3.

3.3. User request for adding new reservoirs to RAT

When data is not available over a reservoir location shown in the RAT framework, jQuery allows a user to push a request button (shown in Figure 16 of the RAT framework user manual). The user needs to specify the GranD ID of the reservoir when sending the request and other information, as mentioned in the user manual (see Figure 16 of the user manual). The form can also be accessed through this link: https://forms.gle/MUebn4bheie1b91J7. The request will push notifications to the administrator of the RAT framework to take further action.

After being notified, the administrator can review the request to add the missing dam to the available list for calculation of reservoir state. During regular monitoring of reservoirs, the newly added reservoir will be considered for deriving all the parameters (including AEC extraction) and the user notified of the availability of data.

4. Results and discussion

The developed RAT software framework was applied in estimating reservoir storage change, inflow, and outflow. Reservoir Inflow and storage change were compared against in-situ measured data. The reservoir outflow was derived from the inflow and storage change using the mass balance approach discussed in section 2.1. Thus, it is assumed that accuracy of reservoir outflow is dependent on inflow and storage-change accuracy.

4.1. Accuracy of reservoir storage change

In-situ measurements of daily reservoir storage were web-scraped from the Central Water Commission (CWC - http://cwc.gov.in/) of India. This web-scraping is very similar in nature to a hydrologic platform development work described by Biswas and Hossain (2018). A map showing the reservoirs' locations along with their surface area (in different colors) and area-perimeter ratio (termed as irregularity index, shown in different colors) is shown in Fig. 7. To quantify the proposed framework's performance for different sizes of reservoirs, 77 reservoirs were classified according to their surface areas (from GranD database) in five different classes (very small, small, medium, large, and very large), as seen in Table 2.

To compare the simulated storage change based on reservoir shape, the reservoirs were classified according to the ratio of surface area to the perimeter (from GranD database), which is termed here as irregularity index. The categories based on area-perimeter ratio are highly irregular, very irregular, irregular, regular, very regular, and highly regular. Details about the classification based on the area-perimeter ratio are shown in Table 3. Three reservoirs, each with a distinctive irregular-

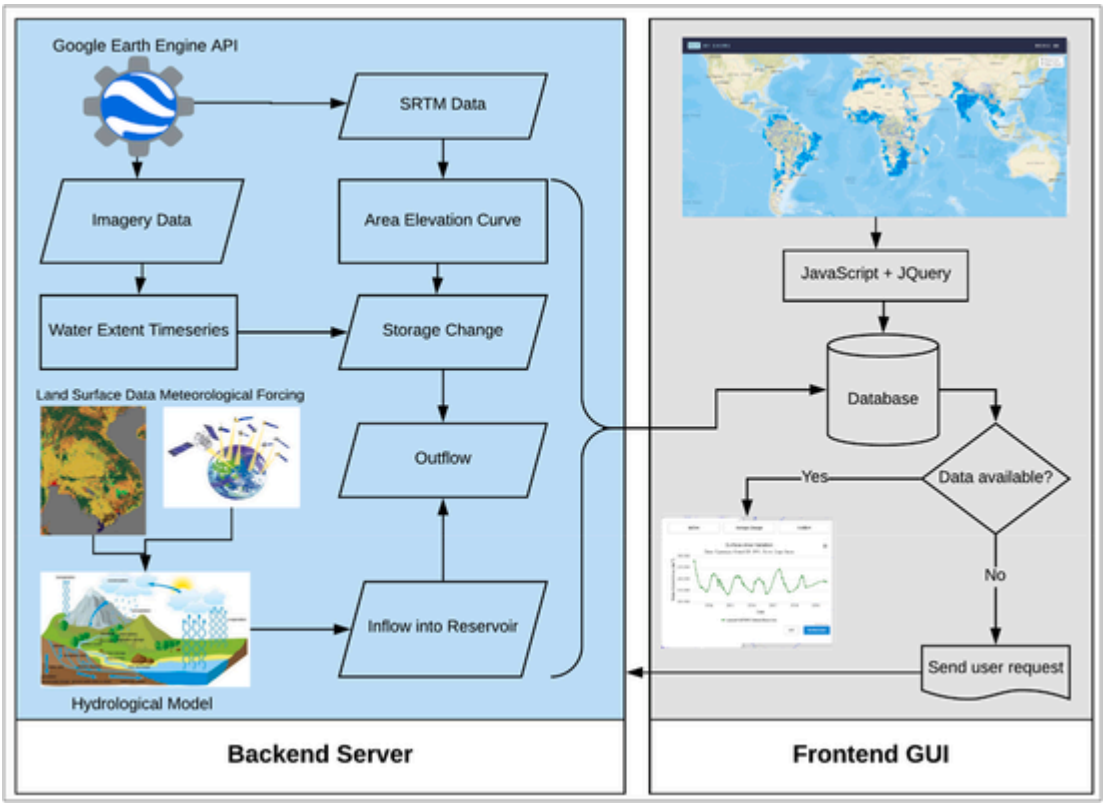

Fig. 6. Data and information exchange between the backend server and the frontend interface. Left panel: Processing of different datasets and simulations. Right panel: summary of datasets that are made available in the frontend.

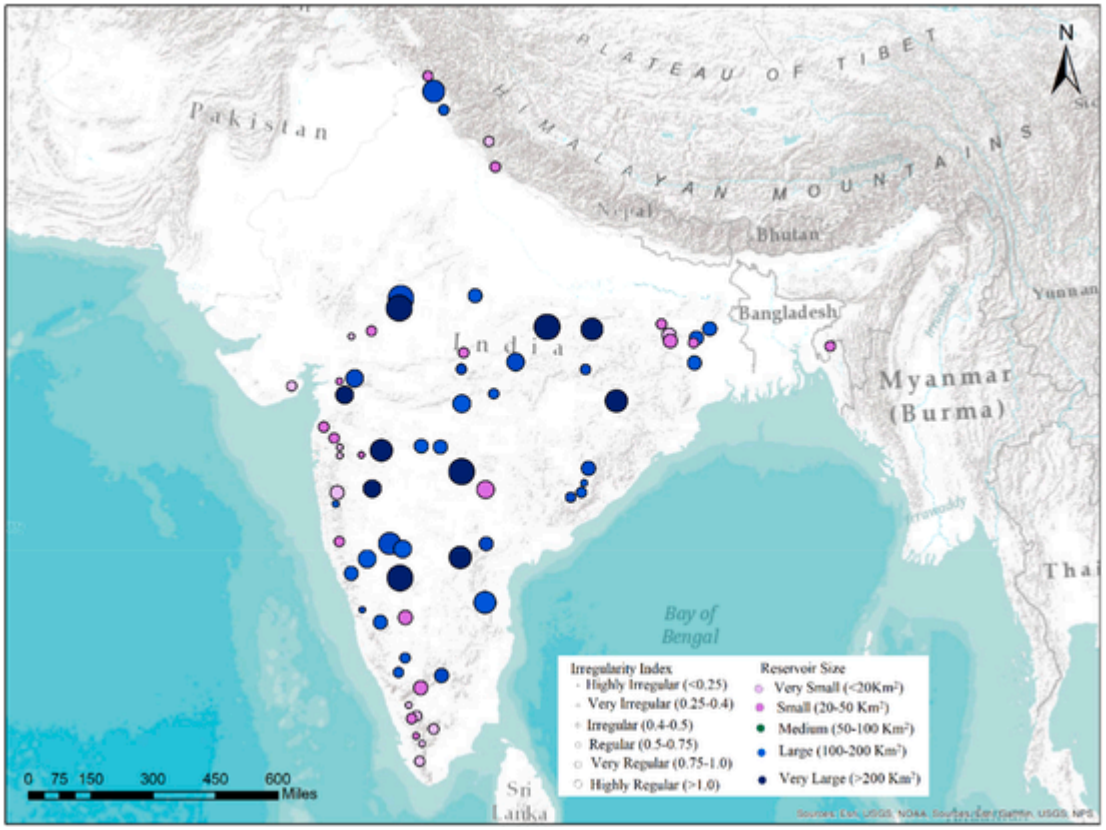

Fig. 7. Validation stations along with the reservoir area, with their sizes color-coded and irregularity index as defined by A/P ratio (in parenthesis).

Table 2
Reservoir classifications according to size for validation of the RAT software tool.

Classification	GranD Area Range (Km^2)	Reservoir Count
Very small	Less than 20	12
Small	20–50	20
Medium	50–100	20
Large	100–200	13
Very large	Greater than 200	12

Table 3
Reservoir classification according to irregularity index.

Classification	Irregularity Index (A/P, unit: Km^2/m)	Reservoir Count
Highly irregular	Less than 0.25	13
Very irregular	0.25–0.40	25
Irregular	0.4–0.5	18
Regular	0.5–0.75	9
Very regular	0.75–1.0	7
Highly regular	Greater than 1.0	5

ity index are shown in Fig. 8 to illustrate the differences in reservoir shapes based on the irregularity index.

The simulated storage change was compared against in-situ storage change of the individual reservoir on a monthly basis. Different sensors (Landsat 8, Sentinel 1 and 2) and different index-based methods (i.e., NDWI, MNDWI, WI, AWEI for Landsat 8 and Sentinel 2; Backscatter Coefficient for Sentinel 1) were tested to compare their accuracy. The correlation coefficient and the normalized root mean square error (NRMSE) were used to quantify the accuracy of individual methods and sensors for different reservoir classes. The sensors and methods are described in Table 4.

The mean correlation coefficient and the normalized RMSE comparison of different reservoir sizes are shown in Fig. 9. All of the sensors and methods yield a correlation coefficient of more than 0.7 for all types of reservoirs. The correlation coefficient is highest for reservoirs with more than 200 km^2 of surface area (very large reservoirs). For Landsat (marked as L8 in Fig. 9), all methods yielded a correlation coefficient of more than 0.8, which means more than 80% of the in-situ storage can be represented by the RAT framework. Except for very large reservoirs, the Normalized RMSE comparison revealed that Sentinel 2-generated storage changes are less accurate than those of Landsat or Sentinel 1, possibly because all of the indices were extensively tested for waterbody detection using Landsat data. Sentinel 1 provided better representation than Sentinel 2; however, the accuracy was less than that of Landsat. Although the data from Sentinel 1 was more accurate than that of all other sensors except Landsat, a few unrealistic estimations and a smaller number of samples resulted in a low score. Vegetated inundation, poor quality atmospheric composition during imagery acquisition, and incorrect identification of sand pixels as water are likely some of the underlying issues resulting in the low performance of Sentinel 1 (Martinis et al., 2015). In the case of very small, small, and medium reservoirs, Landsat performed better for all indices than the other two sensors. Among the different methods of Landsat 8, the DSWE method generated time series with continuous underestimation of water area and fewer records compared to the others. This was due to multiple filtering conditions. Additionally, GEE processing time was almost five times higher for DSWE than the calculations of other indices, making GEE a less practical method of global reservoir monitoring. MNDWI method was found to have limited skill for reservoirs located in steep terrains. Compared to all other methods, NDWI produced consistently better results with a simpler processing approach.

The storage change time series also was classified according to reservoir the irregularity index, which was used for very irregularly shaped reservoirs with extensive shorelines. The satellite imageries have limitations in detecting water pixels at the edges; thus, it was helpful to quantify the relative performance of the sensors and methods. The

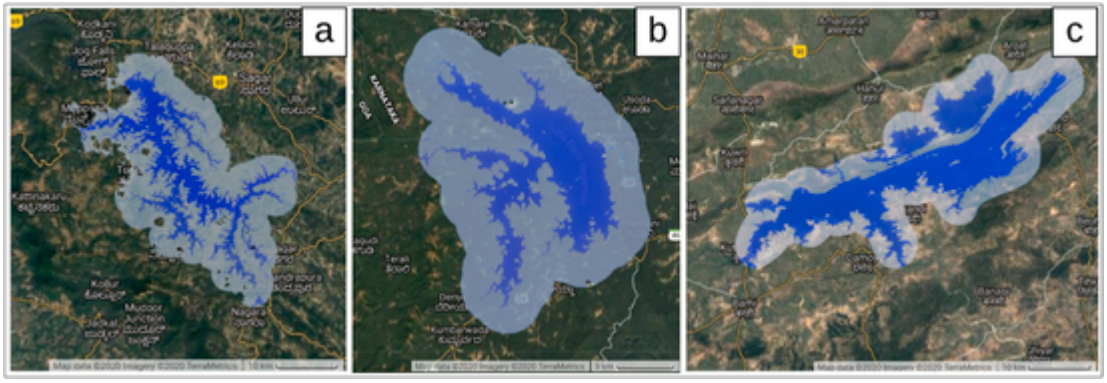

Fig. 8. Reservoirs according to differing irregularity indices: (a) Highly Irregular Linganamakki Reservoir over Sharavathi River, India with A/P ratio 0.19 (Surface area 146.49 km^2), (b) Regular-shaped Supa Reservoir over Kalinadi River, India with A/P ratio 0.51 (Surface area 94 km^2), (c) Highly regular Ban Sagar Reservoir over Sone River, India with A/P ratio of 1.8 (Surface area 384.3 km^2).

Table 4
Sensors, temporal and spatial resolution, and applied methods.

Sensor	Temporal and Spatial Resolution	Method	References
Landsat 8	15 days (30 m)	NDWI	McFeeters (1996)
		MNDWI	Xu (2006)
		WI	Fisher et al. (2016)
		AWEI	Feyisa et al. (2014)
		DSWE	Jones (2019)
Sentinel 1	10 days (10 m)	Backscatter Filter	Ahmad et al. (2019)
Sentinel 2	5 days (10 m)	NDWI	McFeeters (1996)
		MNDWI	Xu (2006)
		WI	Fisher et al. (2016)
		AWEI	Feyisa et al. (2014)
		DSWE	Jones (2019)

mean correlation coefficient and mean of the normalized RMSE for each of the classes were compared and shown in Fig. 10. The accuracy of every method and sensor decreased with the irregularity of the reservoirs. Landsat-based methods worked best for reservoirs in the irregular category. For regular shaped reservoirs, almost all methods yielded similar results. Highly irregular shaped reservoirs returned the lowest correlation coefficient, mostly due to water detection along the reservoirs' shorelines. Considering all the advantages and disadvantages of each of the sensors and methods, the Landsat 8-based NDWI method's performance was found to be most robust and consistent and was therefore selected for the operational RAT software framework.

4.2. Validation of reservoir surface area estimation

The RAT framework's simulated reservoir surface area was compared with the latest published reservoir surface area dataset prepared by Zhao and Gao (2018). Zhao and Gao (2018) dataset provides the surface water extent area of the GranD database from 1984 to 2015 on a monthly scale. We compared the total reservoir surface area (from the NDWI method of Landsat 8 sensor and the DSWE method for Landsat 5) of all the RAT domain reservoirs to the total surface area of the same reservoirs estimated by Zhao and Gao (2018). The RAT framework was extensively validated for the Landsat 8 satellite imagery, and it was found that the NDWI method worked best in the case of the Landsat 8. Due to differences in sensor characteristics and differences in spectral band ranges, we found that the DSWE method worked best for the Landsat 5. For operational purposes, water areas generated from Landsat 5 (using the DSWE method) and Landsat 8 (using the NDWI method) were combined to produce monthly timeseries and then compared with Zhao and Gao (2018) data (Fig. 11). It was also found that reservoir surface area records were discontinuous for many reservoirs in the Zhao and Gao (2018) data during the years before 2000; consequently, comparison began with the year 2000. The proposed framework yielded a correlation coefficient of 0.92. Fig. 11 shows that the reservoir surface area's seasonal variation is more clearly visible when the proposed framework-generated dataset was used. We should note that Zhao and Gao (2018) dataset is not available in near real-time

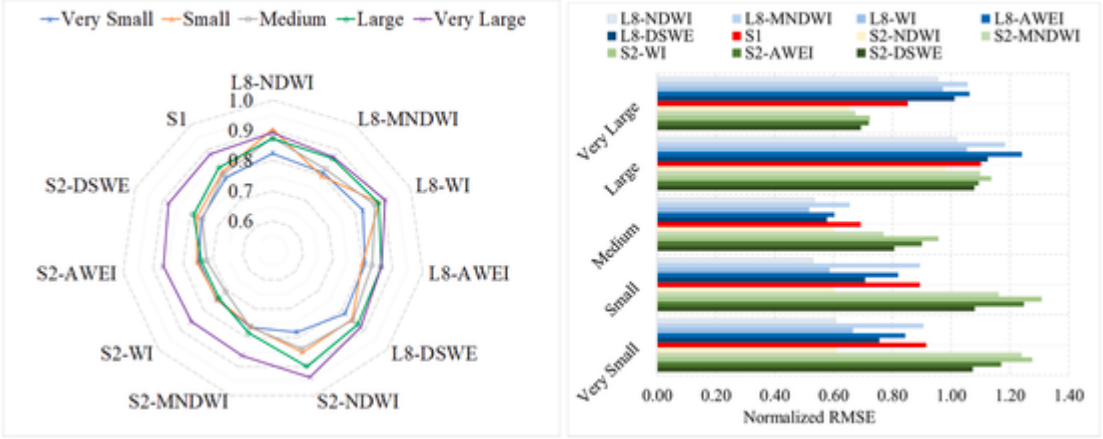

Fig. 9. (left) Correlation Coefficient and (right) Normalized RMSE comparison of reservoirs of various sizes.

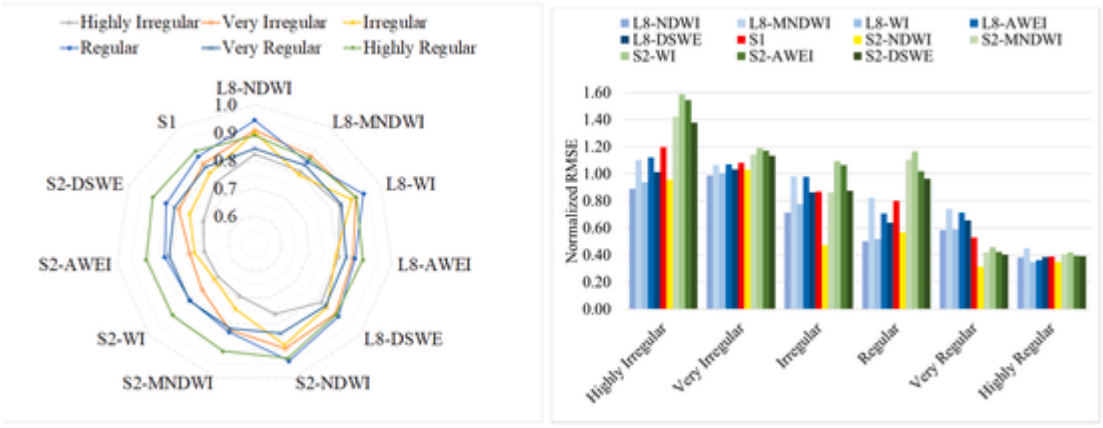

Fig. 10. Correlation Coefficient (left side) and Normalized RMSE comparison of different reservoir classes defined according to the irregularity index (right side).

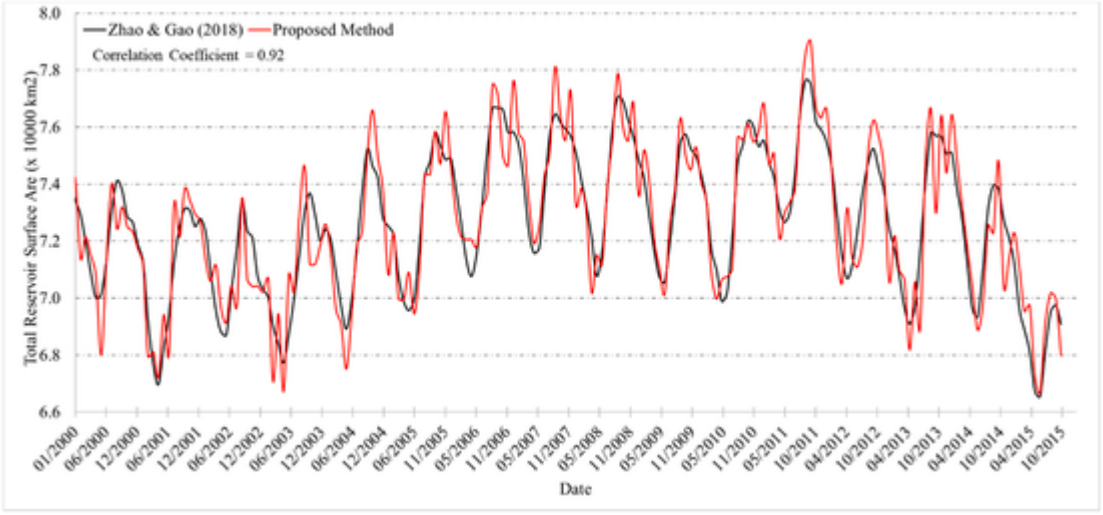

Fig. 11. Comparison between the derived total reservoir surface area of all the reservoirs included in the RAT framework with Zhao and Gao (2018) generated reservoir surface area.

scale for monitoring reservoir dynamics from the latest available satellite imagery.

4.3. Validation of VIC hydrological model

Using the land surface parameters and meteorological forcing mentioned in Section 2.3.4, the VIC and Route model was simulated for the RAT domain (South America, Africa, and Southeast Asia). The simulated daily streamflow was first compared against ground-based daily discharge data collected through different sources. Information about validation stations is mentioned in Table 5. The stations along with the respective basins are shown in the upper panel of Fig. 12.

Time series comparisons of two stations are shown in the middle panel of Fig. 12. The left panel is Tabatinga station, located in the Amazon basin, where the correlation coefficient was less than 0.7, and the VIC model was not very accurate in representing low-flow and high-flow peaks. A similar case was observed at other stations. Time-series comparison of Kampong Cham station located on the Mekong river (shown in the middle right corner) found accuracy was highest for the correlation coefficient. This basin performed exceptionally well due to subbasin scale calibration performed by Hossain et al. (2017). Nevertheless, the hydrological model showed dry season flow to be lower than the actual flow and overestimated the peaks. Summary statistics of all validation stations are shown in the lower panel of Fig. 12. In Southeast Asia's stations, the correlation coefficients were more than 0.8, whereas the South American stations showed more than 0.6. Also, in some stations, NRMSE was higher with a good correlation coefficient due to the model's underperformance in capturing seasonality. We found that flow-direction modification improved the results significantly.

4.4. Comparison of streamflow with GRADES streamflow

We compared streamflow at different inflow locations with the Global Reach-level A priori Discharge Estimates for Surface Water and Ocean Topography modeled streamflow (GRADES; Lin et al., 2019). We compared our model's estimated streamflow with the GRADES model's simulated streamflow at 44 randomly chosen locations along the river reaches within the RAT domain. The summary statistics are shown in Fig. 13. The average correlation coefficient of all the stations was 0.62, and the mean of normalized root mean square error was 0.49. Again, stations located in Southeast Asia performed better compared to the stations in the South America region. This is a clear indication that better calibration at regional and basin scales can improve simulated streamflow accuracy at the locations where our model underperformed.

Table 5
VIC hydrological model validation stations (BWDB: Bangladesh Water Development Board, Bangladesh; MRC: Mekong River Commission; CWC: Central Water Commission, India; GRDC: Global Runoff Data Center; PWAPDA: Pakistan Water and Power Development Authority; and So-Hybam: HYBAM monitoring program- https://hybam.obs-mip.fr/).

Station	Basin	Longitude	Latitude	Data Source	Data Availability
Hardinge Bridge	Ganges	89.0273	24.0649	BWDB	2001–2019
Bahadurabad	Brahmaputra	89.7161	25.3363	BWDB	2001–2019
Kampong Cham	Mekong	105.4740	11.9855	MRC	2001–2019
Vijayawada	Krishna	80.6091	16.5049	CWC	2007–2019
Polavaram	Godavari	81.6547	17.2575	CWC	2001–2019
Pye	Irrawardy	95.2123	18.8075	GRDC	2001–2010
Hyderabad	Indus	68.3111	25.3727	PWAPDA	2014–2019
Katima Mulilo	Zambezi	24.2809	−17.4843	GRDC	2001–2018
Vioolsdrif	Orange	17.7295	−28.7611	GRDC	2001–2018
Lokoja	Niger	6.7571	7.7595	GRDC	2001–2006
Brazzaville	Congo	15.2817	−4.2904	So-Hybam	2001–2020
Obidos	Amazon	−55.5178	−1.9339	So-Hybam	2001–2018
Chapeton	Rio Parana	−60.3540	−31.6236	GRDC	2001–2014
Pichi Mahuida	Rio Colorado	−64.8295	−38.8261	GRDC	2001–2014
Primera Angostura	Rio Negro	−63.6744	−40.4452	GRDC	2001–2015
Bhairab Bazar	Meghna	90.9937	24.0441	BWDB	2001–2019
Serrinha	Amazon	−64.8077	−0.4891	So-Hybam	2001–2019
Tabatinga	Amazon	−69.9429	−4.2832	So-Hybam	2006–2016
Ocona	Rio Ocona	−72.6795	−16.7330	GRDC	2006–2018
La Pascana	Rio Tambo	−70.133	−18.4940	GRDC	2001–2018
Haindi	Saint Paul	−10.1238	6.5698	GRDC	2012–2019
Ruacana	Kunene	11.9861	−16.7715	GRDC	2001–2018
Beibrug	Limpopo	30.1731	−23.1643	GRDC	2001–2019
Prieska	Orange	22.7492	−30.0171	GRDC	2001–2018
Gamtoos Poort	Gamptoos	25.9853	−34.3954	GRDC	2001–2018

5. Conclusion and future scope

To our knowledge, the online software framework for reservoir monitoring called RAT is the first of its kind. Given that the RAT tool is now publicly available for the world to use and benefit from, we believe the following are some examples of potential applications of this framework.

- By using this tool, long-term records denoting real-time behavior and operating rules at reservoirs can become publicly available.
- RAT can help users and the scientific community derive a global picture of reservoir monitoring, how they are being operated, and how they are likely impacting natural river flow and its variability as a function of climate, hydrologic regime, and socio-economic indicators.
- With further improvements in hydrological modeling using locally available ground observations, the RAT framework can be used with higher accuracy in local, regional, and global scale operational water resources management considering its near real-time data availability.
- The RAT framework can facilitate feasibility study of proposed/planned dams. It can be used to estimate the future reservoir capacity and inflow availability at any location, which is useful in optimizing reservoir benefits.
- The RAT framework presents future possibilities to study the impact of harnessing hydropower on river temperature, greenhouse gas emissions, aquatic habitats, land-use and landcover change, and agriculture practices.
- The RAT tool can be used to minimize conflict between riparian countries (i.e., Egypt and Ethiopia over Nile Basin; China, India, and Bangladesh over Ganges-Brahmaputra-Meghna Basin; China, Laos, Thailand, Cambodia, Vietnam over Mekong Basin) as it can be considered an unbiased tool to all parties and provide data needed to drive fair and transparent water-sharing agreements.

There are some future improvements that can be considered to make the framework more applicable in solving real-world water challenges. While the hydrological model validation showed promise, known uncertainties mandate that current results be carefully interpreted. Additionally, the VIC model used here will still need time to be improved and validated further at a more granular level. This need for improvement at many regions is evident when a superior goodness-of-fit such as Nash-Sutcliffe efficiency (Fig. 14) is compared with in-situ flow (accumulated over 16 days to match Landsat revisit time and for reservoir management). Improved reservoir inflow estimation can be made by using regional and basin-scale calibration, and validation of the hydrological model is one of them. The more complex method of water pixel identification from satellite imagery with artificial intelligence and the application of machine learning algorithms may yield better estimation of reservoir surface area. Reservoir bathymetry data from ground surveying or Lidar applications may be used to define the area-elevation curve more accurately. Lastly, reservoir outflow calculated in this study includes all types of diversions and consumptive water uses for various purposes, which may not be very accurate nor comparable to the actual reservoir releases. Thus, the simulated outflow should be compared with measured flow at in-situ locations immediately downstream of a reservoir.

The focus of our study here was on reservoirs and on methods of enabling the monitoring/prediction of reservoir states (surface area, storage change, inflow and outflow) at weekly to monthly scales of reservoir management. It should be noted that our study is not about developing a global hydrological modeling framework or even promoting an existing one for that matter. Our RAT framework is agnostic enough that the current hydrological model (VIC) can be replaced with other competing hydrological models. Our work to develop such an open and publicly available tool is driven by our mission to democratize water information on regulated river basins for all stakeholders and to facilitate more equitable water management. We believe that such a tool can level the playing field for stakeholder agencies and riparian nations that suffer from limited access to information on water availability due to hydro-politics, lack of in-situ infrastructure, or low adaptive capacity.

Software availability

https://github.com/nbiswasuw/rat-reservoir_assessment_tool.

Key findings

1. A web-based framework was developed for near-realtime monitoring and impact analysis of reservoirs around the world.
2. The framework is freely available and able to monitor the dynamic state for more than 1500 reservoirs.
3. The storage changes of more than seventy-five percent of reservoirs were accurately captured with skillful inflow simulation at bi-weekly timescale.

Declaration of competing interest

The authors declare that they have no known competing financial interests or personal relationships that could have appeared to influence the work reported in this paper.

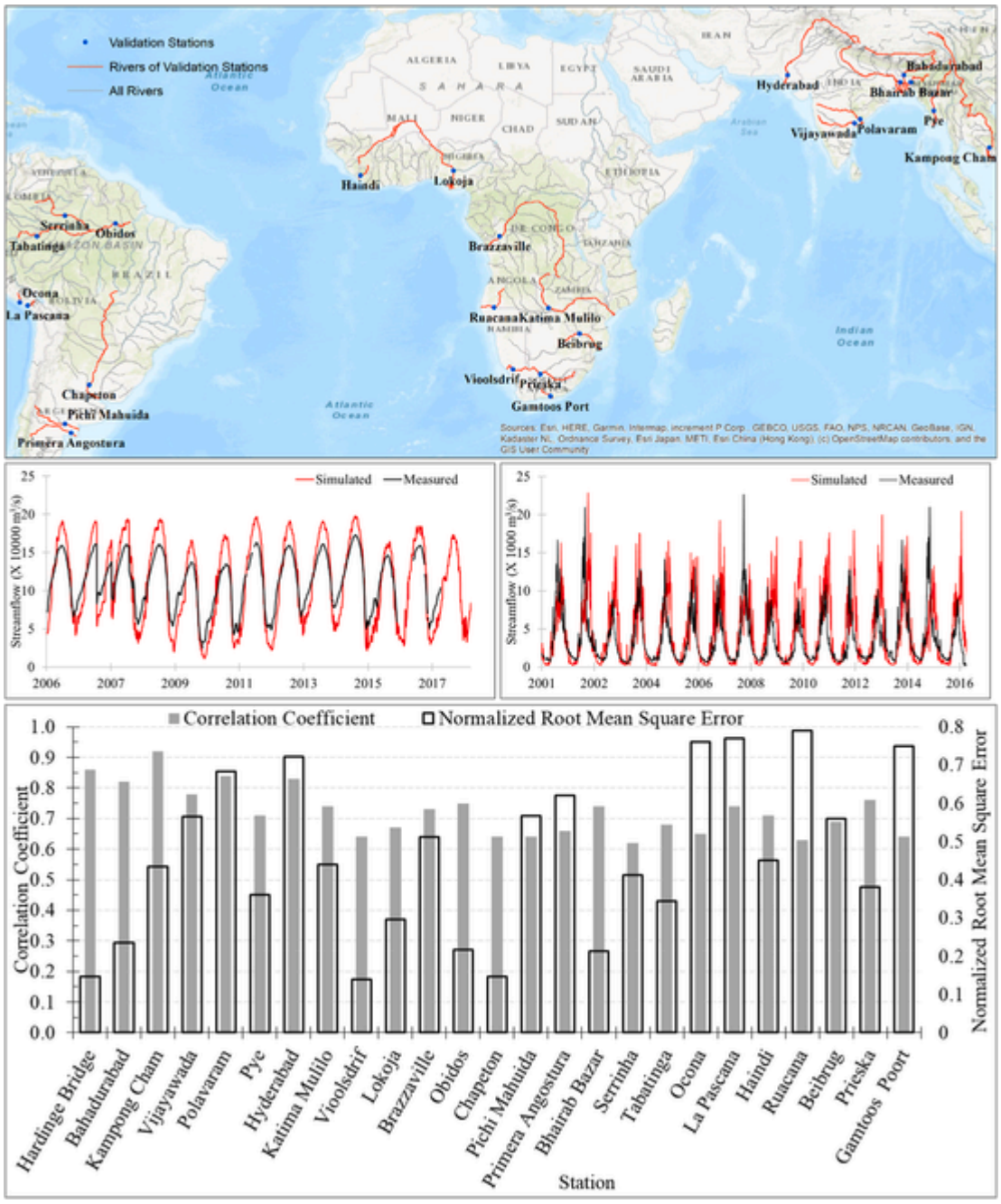

Fig. 12. (upper panel) VIC Model validation stations along with the respective basins, (center left) Streamflow timeseries of Tabatinga station of Amazon Basin, (center right) Streamflow Kampong Cham station of Mekong Basin, (lower panel) Summary statistics of validation stations.

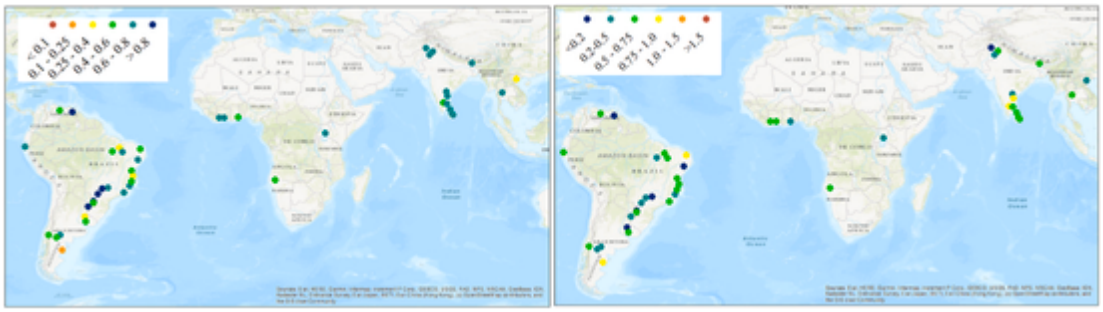

Fig. 13. (left) Correlation Coefficient and (right) Normalized RMSE of different stations compared with GRADES simulated streamflow.

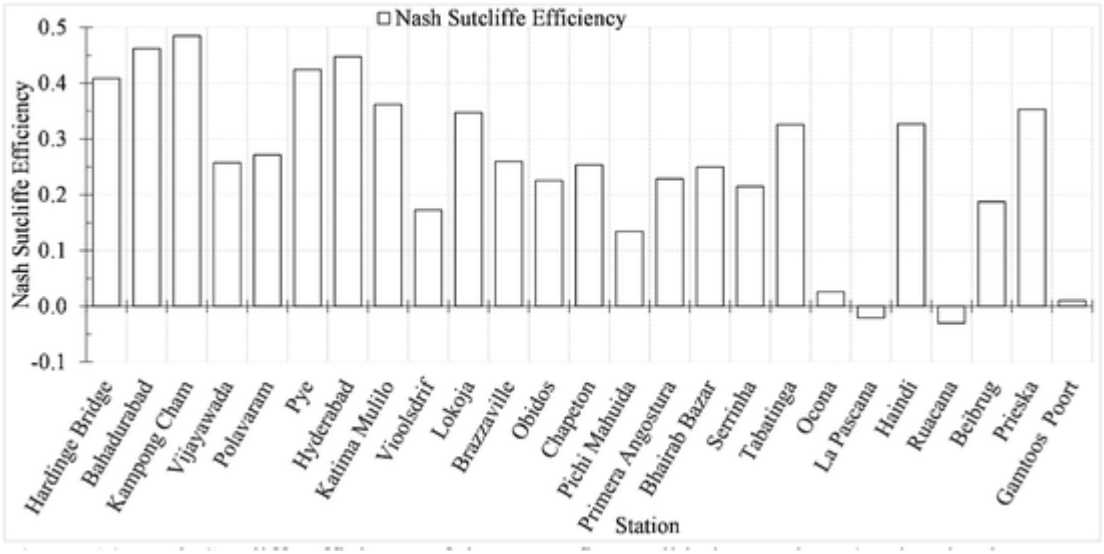

Fig. 14. Nash-Sutcliffe efficiency of the streamflow validation stations (against in-situ stream flow) shown at 16-day aggregation in accordance with Landsat revisit period and reservoir management.

Acknowledgments

This work was supported by a NASA Applied Science Program grant in Water Resources NNX15AC63G and NNX16AQ54G. Additional support from NASA Applied Sciences SERVIR grant 80 NSSC20K0152 is also acknowledged.

Appendix A. Supplementary data

Supplementary data to this article can be found online at https://doi.org/10.1016/j.envsoft.2021.105043.

Uncited references

WCD, 2000.

References

Ahmad, S.K., Hossain, F., Eldardiry, H., Pavelsky, T.M., 2019. A fusion approach for water area classification using visible, near infrared and synthetic aperture radar for South asian conditions. IEEE Trans. Geosci. Rem. Sens. 58 (4), 2471–2480. https://doi.org/10.1109/TGRS.2019.2950705.

Alsdorf, D.E., Rodríguez, E., Lettenmaier, D.P., 2007. Measuring surface water from space. Rev. Geophys. 45, RG2002. https://doi.org/10.1029/2006RG000197.

Avisse, N., Tilmant, A., Müller, M.F., Zhang, H., 2017. Monitoring small reservoirs' storage with satellite remote sensing in inaccessible areas. Hydrol. Earth Syst. Sci. 21, 6445–6459. https://doi.org/10.5194/hess-21-6445-2017.

Barbarossa, V., Huijbregts, M.A., Beusen, A.H., Beck, H.E., King, H., Schipper, A. M., 2018. FLO1K, global maps of mean, maximum and minimum annual streamflow at 1 km resolution from 1960 through 2015. Scientific data 5, 180052. https://doi.org/10.1038/sdata.2018.52.

Bierkens, M.F.P., Bell, V.A., Burek, P., Chaney, N., Condon, L., David, C.H., de Roo, A., Döll, P., Drost, N., Famiglietti, J.S., Flörke, M., Gochis, D.J., Houser, P., Hut, R., Keune, J., Kollet, S., Maxwell, R., Reager, J.T., Samaniego, L., Sudicky, E., Sutanudjaja, E.H., van de Giesen, N., Winsemius, H., Wood, E.F., 2015. Hyper-resolution global hydrological modelling: what is next?. Hydrol. Process. 29, 310–320. https://doi.org/10.1002/hyp.10391.

Biswas, N.K., Hossain, F., 2018. A scalable open-source web-analytic framework to improve satellite-based operational water management in developing countries. J. Hydroinf. 20 (1), 49–68. https://doi.org/10.2166/hydro.2017.073.

Biswas, N.K., Hossain, F., Bonnema, M., Okeowo, M.A., Lee, H., 2019. An altimeter height extraction technique for dynamically changing rivers of South and South-East Asia. Remote Sens. Environ. 221, 24–37. https://doi.org/10.1016/j.rse.2018.10.033.

Bonnema, M., Hossain, F., 2017. Inferring reservoir operating patterns across the Mekong Basin using only space observations. Water Resour. Res. 53 (5), 3791–3810. https://doi.org/10.1002/2016WR019978.

Bonnema, M., Sikder, S., Miao, Y., Chen, X., Hossain, F., Ara Pervin, I., Mahbubur Rahman, S.M., Lee, H., 2016. Understanding satellite-based monthly-to-seasonal reservoir outflow estimation as a function of hydrologic controls. Water Resour. Res. 52 (5), 4095–4115. https://doi.org/10.1002/2015WR017830.

Bunn, S.E., Arthington, A.H., 2002. Basic principles and ecological consequences of altered flow regimes for aquatic biodiversity. Environ. Manag. 30 (4), 492–507. https://doi.org/10.1007/s00267-002-2737-0.

Degu, A.M., Hossain, F., Niyogi, D., Pielke Sr, R., Shepherd, J.M., Voisin, N., Chronis, T., 2011. The influence of large dams on surrounding climate and precipitation patterns. Geophysical Research Letters. Geophys. Res. Lett. 38 (4). https://doi.org/10.1029/2010GL046482.

Döll, P., Fiedler, K., Zhang, J., 2009. Global-scale analysis of river flow alterations due to water withdrawals and reservoirs. Hydrol. Earth Syst. Sci. 13 (12), 2413–2432. https://doi.org/10.5194/hess-13-2413-2009.

Döll, P., Kaspar, F., Lehner, B., 2003. A global hydrological model for deriving water availability indicators: model tuning and validation. J. Hydrol. 270 (1–2), 105–134. https://doi.org/10.1016/S0022-1694(02)00283-4.

Eldardiry, H., Hossain, F., 2019. Understanding reservoir operating rules in the transboundary nile river basin using macroscale hydrologic modeling with satellite measurements. J. Hydrometeorol. 20 (11), 2253–2269. https://doi.org/10.1175/JHM-D-19-0058.1.

Fatichi, S., Vivoni, E.R., Ogden, F.L., Ivanov, V.Y., Mirus, B., Gochis, D., Downer, C.W., Camporese, M., Davison, J.H., Ebel, B., Jones, N., 2016. An overview of current applications, challenges, and future trends in distributed process-based models in hydrology. J. Hydrol. 537, 45–60. https://doi.org/10.1016/j.jhydrol.2016.03.026.

Feyisa, G.L., Meilby, H., Fensholt, R., Proud, S.R., 2014. Automated Water Extraction Index: a new technique for surface water mapping using Landsat imagery. Remote Sens. Environ. 140, 23–35. https://doi.org/10.1016/j.rse.2013.08.029.

Fisher, A., Flood, N., Danaher, T., 2016. Comparing Landsat water index methods for automated water classification in eastern Australia. Remote Sens. Environ. 175, 167–182. https://doi.org/10.1016/j.rse.2015.12.055.

Funk, C., Peterson, P., Landsfeld, M., Pedreros, D., Verdin, J., Shukla, S., Husak, G., Rowland, J., Harrison, L., Hoell, A., Michaelsen, J., 2015. The climate hazards infrared precipitation with stations- a new environmental record for monitoring extremes. Scientific data 2, 150066. https://doi.org/10.1038/sdata.2015.66.

Gao, H., 2015. Satellite remote sensing of large lakes and reservoirs: from elevation and area to storage. Wiley Interdiscip. Rev. Water 2 (2), 147–157. https://doi.org/10.1002/wat2.1065.

Gao, H., Birkett, C., Lettenmaier, D.P., 2012. Global monitoring of large reservoir storage from satellite remote sensing. Water Resour. Res. 48 (9), 1–12. https://doi.org/10.1029/2012WR012063.

Gebregiorgis, A., Hossain, F., 2011. How much can a priori hydrologic model predictability help in optimal merging of satellite precipitation products?. J. Hydrometeorol. 12 (6), 1287–1298. https://doi.org/10.1175/JHM-D-10-05023.1.

Geological Survey, U. S, 1997. Global Land Cover Characteristics Data Base. http://Edc2.Usgs.Gov/Glcc/Globe_Int.Php.

Gorelick, N., Hancher, M., Dixon, M., Ilyushchenko, S., Thau, D., Moore, R., 2017. Google earth engine: planetary-scale geospatial analysis for everyone. Remote Sens. Environ. 202, 18–27. https://doi.org/10.1016/j.rse.2017.06.031.

Grill, G., Lehner, B., Lumsdon, A.E., Macdonald, G.K., Zarfl, C., Reidy Liermann, C., 2015. An index-based framework for assessing patterns and trends in river

fragmentation and flow regulation by global dams at multiple scales. Environ. Res. Lett. 10 (1), 015001. https://doi.org/10.1088/1748-9326/10/1/015001.
Hanasaki, N., Kanae, S., Oki, T., 2006. A reservoir operation scheme for global river routing models. J. Hydrol. 327 (1–2), 22–41. https://doi.org/10.1016/j.jhydrol.2005.11.011.
Hennig, T.A., Kretsch, J.L., Pessagno, C.J., Salamonowicz, P.H., Stein, W.L., 2001. The shuttle radar topography mission. In: Lecture Notes in Computer Science (Including Subseries Lecture Notes in Artificial Intelligence and Lecture Notes in Bioinformatics). https://doi.org/10.1007/3-540-44818-7_11.
Hossain, F., Sikder, S., Biswas, N., Bonnema, M., Lee, H., Luong, N.D., Hiep, N. H., Du Duong, B., Long, D., 2017. Predicting water availability of the regulated Mekong river basin using satellite observations and a physical model. Asian J. Water Environ. Pollut. 14 (3), 39–48. https://doi.org/10.3233/AJW-170024.
Hossain, F., Katiyar, N., Wolf, A., Hong, Y., 2007. The emerging role of satellite rainfall data in improving the hydro-political situation of flood monitoring in the under-developed Regions of the world. Nat. Hazards 43, 199–210. https://doi.org/10.1007/s11069-006-9094-x.
Iqbal, N., Hossain, F., Lee, H., Akhter, G., 2017. Integrated groundwater resource management in Indus Basin using satellite gravimetry and physical modeling tools. Environ. Monit. Assess. 189 (3), 128. https://doi.org/10.1007/s10661-017-5846-1.
Jones, J.W., 2019. Improved automated detection of subpixel-scale inundation-revised Dynamic Surface Water Extent (DSWE) partial surface water tests. Rem. Sens. 11 (4), 374. https://doi.org/10.3390/rs11040374.
Khaki, M., Hendricks Franssen, H.J., Han, S.C., 2020. Multi-mission satellite remote sensing data for improving land hydrological models via data assimilation. Nat. Sci. Rep. 10, 18791. https://doi.org/10.1038/s41598-020-75710-5.
Kansakar, P., Hossain, F., 2016. A review of applications of satellite earth observation data for global societal benefit and stewardship of planet earth. Space Pol. 36, 46–54. https://doi.org/10.1016/j.spacepol.2016.05.005.
Khan, O., Mwelwa-Mutekenya, E., Crosato, A., Zhou, Y., 2014. Effects of dam operation on downstream river morphology: the case of the middle Zambezi River. Proc. Inst. Civil Eng. Water Manag. 167 (10), 585–600.
Khattar, R., Ames, D.P., 2020. A web services based water data sharing approach using open geospatial consortium standards. Open Water J. 6 (1).
Lauri, H., De Moel, H., Ward, P.J., Räsänen, T.A., Keskinen, M., Kummu, M., 2012. Future changes in Mekong River hydrology: impact of climate change and reservoir operation on discharge. Hydrol. Earth Syst. Sci.. https://doi.org/10.5194/hess-16-4603-2012.
Lehner, B., Liermann, C.R., Revenga, C., Vörömsmarty, C., Fekete, B., Crouzet, P., Döll, P., Endejan, M., Frenken, K., Magome, J., Nilsson, C., 2011. High-resolution mapping of the world's reservoirs and dams for sustainable river-flow management. Front. Ecol. Environ. 9 (9), 494–502. https://doi.org/10.1890/100125.
Liang, X., Lettenmaier, D.P., Wood, E.F., Burges, S.J., 1994. A simple hydrologically based model of land surface water and energy fluxes for general circulation models. J. Geophys. Res.: Atmosphere 99 (D7), 14415–14428. https://doi.org/10.1029/94jd00483.
Lin, P., Pan, M., Beck, H.E., Yang, Y., Yamazaki, D., Frasson, R., et al., 2019. Global reconstruction of naturalized river flows at 2.94 million reaches. Water Resour. Res. 55 (8), 6499–6516.
Lohmann, D., Raschke, E., Nijssen, B., Lettenmaier, D.P., 1998. Regional scale hydrology: I. Formulation of the VIC-2L model coupled to a routing model. Hydrol. Sci. J. 43 (1), 131–141. https://doi.org/10.1080/02626669809492107.
Lugg, A., Copeland, C., 2014. Review of cold water pollution in the Murray–Darling Basin and the impacts on fish communities. Ecol. Manag. Restor. 15 (1), 71–79. https://doi.org/10.1111/emr.12074.
Martinis, S., Kuenzer, C., Wendleder, A., Huth, J., Twele, A., Roth, A., Dech, S., 2015. Comparing four operational SAR-based water and flood detection approaches. Int. J. Rem. Sens. 36 (13), 3519–3543. https://doi.org/10.1080/01431161.2015.1060647.
McFeeters, S.K., 1996. The use of the Normalized Difference Water Index (NDWI) in the delineation of open water features. Int. J. Rem. Sens. 17 (7), 1425–1432. https://doi.org/10.1080/01431169608948714.
Meigh, J.R., McKenzie, A.A., Sene, K.J., 1999. A grid-based approach to water scarcity estimates for eastern and southern Africa. Water Resour. Manag. 13 (2), 85–115. https://doi.org/10.1023/A:1008025703712.
Mishra, V., Shah, H.L., 2018. Hydroclimatological perspective of the Kerala flood of 2018. J. Geol. Soc. India 92 (5), 645–650. https://doi.org/10.1007/s12594-018-1079-3.
Nachtergaele, F., Van Velthuizen, H., Verelst, L., Batjes, N., Dijkshoorn, K., Van Engelen, V., et al., 2008. Harmonized World Soil Database–. Food and Agriculture Organization of the United Nations.
Nijssen, B., O'donnell, G.M., Hamlet, A.F., Lettenmaier, D.P., 2001a. Hydrologic sensitivity of global rivers to climate change. Climatic Change 50 (1–2), 143–175. https://doi.org/10.1023/A:1010616428763.
Nijssen, B., O'Donnell, G.M., Lettenmaier, D.P., Lohmann, D., Wood, E.F., 2001b. Predicting the discharge of global rivers. J. Clim. 14 (15), 3307–3323. https://doi.org/10.1175/1520-0442(2001)014<3307:PTDOGR>2.0.CO;2.
Pekel, J.F., Cottam, A., Gorelick, N., Belward, A.S., 2016. High-resolution mapping of global surface water and its long-term changes. Nature 540 (7633), 418. https://doi.org/10.1038/nature20584.
Poff, N.L., Zimmerman, J.K.H., 2010. Ecological responses to altered flow regimes: a literature review to inform the science and management of environmental flows. Freshw. Biol. 55 (1). https://doi.org/10.1111/j.1365-2427.2009.02272.x.
Pokhrel, Y.N., Fan, Y., Miguez-Macho, G., 2014. Potential hydrologic changes in the Amazon by the end of the 21st century and the groundwater buffer. Environ. Res. Lett. 9 (8), 084004. https://doi.org/10.1088/1748-9326/9/8/084004.
Siddique-E-Akbor, A.H.M., Hossain, F., Sikder, S., Shum, C.K., Tseng, S., Yi, Y., Turk, F.J., Limaye, A., 2014. Satellite precipitation data–driven hydrological modeling for water resources management in the Ganges, Brahmaputra, and Meghna Basins. Earth Interact. 18 (17), 1–25. https://doi.org/10.1175/EI-D-14-0017.1.
Sikder, M.T., Elahi, K.M., 2013. Environmental degradation and global warming-consequences of Himalayan mega dams. Am. J. Environ. Protect. 2 (1), 1–9. https://doi.org/10.11648/j.ajep.20130201.11.
Solander, K.C., Reager, J.T., Famiglietti, J.S., 2016a. How well will the Surface Water and Ocean Topography (SWOT) mission observe global reservoirs?. Water Resour. Res. 52 (3), 2123–2140. https://doi.org/10.1002/2015WR017952.
Solander, K.C., Reager, J.T., Thomas, B.F., David, C.H., Famiglietti, J.S., 2016b. Simulating human water regulation: the development of an optimal complexity, climate-adaptive reservoir management model for an LSM. J. Hydrometeorol. 17 (3), 725–744. https://doi.org/10.1175/JHM-D-15-0056.1.
Strobl, E., Strobl, R.O., 2011. The distributional impact of large dams: evidence from cropland productivity in Africa. J. Dev. Econ. 96 (2), 432–450 (November).
Voisin, N., Li, H., Ward, D., Huang, M., Wigmosta, M., Leung, L.R., 2013. On an improved sub-regional water resources management representation for integration into earth system models. Hydrol. Earth Syst. Sci. 17 (9), 3605–3622. https://doi.org/10.5194/hess-17-3605-2013.
WCD, 2000. Dams and Development: a New Framework for Decision-Making. Earthscan Publications, London, UK.
Wood, E.F., et al., 2011. Hyperresolution global land surface modeling: meeting a grand challenge for monitoring Earth's terrestrial water. Water Resour. Res. 47, W05301. https://doi.org/10.1029/2010WR010090.
Woldemichael, A.T., Hossain, F., Pielke, R., Beltrán-Przekurat, A., 2012. Understanding the impact of dam-triggered land use/land cover change on the modification of extreme precipitation. Water Resour. Res. 48 (9). https://doi.org/10.1029/2011WR011684.
World Bank Water in agriculture https://www.worldbank.org/en/topic/water-in-agriculture 2020 s29 December 2020
Wu, H., Kimball, J.S., Mantua, N., Stanford, J., 2011. Automated upscaling of river networks for macroscale hydrological modeling. Water Resour. Res. 47 (3). https://doi.org/10.1029/2009WR008871.
Xu, H., 2006. Modification of normalised difference water index (NDWI) to enhance open water features in remotely sensed imagery. Int. J. Rem. Sens. 27 (14), 3025–3033. https://doi.org/10.1080/01431160600589179.
Zarfl, C., Lumsdon, A.E., Berlekamp, J., Tydecks, L., Tockner, K., 2014. A global boom in hydropower dam construction. Aquat. Sci. 77 (1), 161–170. https://doi.org/10.1007/s00027-014-0377-0.
Zhao, G., Gao, H., 2018. Automatic correction of contaminated images for assessment of reservoir surface area dynamics. Geophys. Res. Lett. 45 (12), 6092–6099. https://doi.org/10.1029/2018GL078343.